Biogeosciences, 5, 1–12, 2008
www.biogeosciences.net/5/1/2008/

Biogeosciences

Distribution and fluxes of aggregates $>100\,\mu$m in the upper kilometer of the South-Eastern Pacific

L. Guidi[1,2], **G. Gorsky**[1], **H. Claustre**[1], **J. C. Miquel**[3], **M. Picheral**[1], **and L. Stemmann**[1]

[1]Université Pierre et Marie Curie-Paris 6, Laboratoire d'Oc'eanographie de Villefranche; CNRS, Laboratoire d'Oc'eanographie de Villefranche, Villefranche-sur-Mer, France
[2]Department of Oceanography, Texas A and M University, College Station, USA
[3]IAEA Marine Environment Laboratory, Monaco

Received: 3 December 2007 – Published in Biogeosciences Discuss.: 20 February 2008
Revised: 7 August 2008 – Accepted: 13 August 2008 – Published:

Abstract. Large sinking particles transport organic and inorganic matter into the deeper layers of the oceans. Between 70 and 90% of the aggregates exported from the surface mixed layer are disaggregated within the upper 1000 m. This decrease with depth indicates that fragmentation and remineralization processes are intense during sedimentation. Generally, the estimates of vertical flux rely on sediment trap data but difficulties inherent in their design limit the reliability of this information. During the BIOSOPE study in the south-eastern Pacific, 76 vertical casts using the Underwater Video Profiler (UVP) and deployments of drifting sediment traps provided an opportunity to fit the UVP data to sediment trap flux measurements. We applied the calculated UVP flux in the upper 1000 m to the whole 8000 km BIOSOPE transect. Comparison between the large particulate material (LPM) abundance and the estimated fluxes from both UVP and sediment traps showed different patterns in different regions. On the western end of the BIOSOPE section the standing stock of particles in the surface layer was high but the export between 150 and 250 m was low. Below this layer the flux values increased. High values of about 30% of the calculated UVP maximum surface zone flux were observed below 900 m at the HNLC station. The South Pacific Gyre exported about $2\,\mathrm{mg\,m^{-2}\,d^{-1}}$. While off Chilean coast 95% of the surface mixed layer matter was disaggregated, remineralized or advected in the upper kilometer, 20% of the surface zone flux was observed below 900 m near the Chilean coast. These results suggest that the export to deep waters is spatially heterogeneous and related to the different biotic and abiotic factors.

Correspondence to: G. Gorsky
(gorsky@obs-vlfr.fr)

1 Introduction

The biological pump is the sum of biological processes by which atmospheric CO_2 fixed in photosynthesis is transferred from the euphotic layer to the ocean interior. Organic and inorganic matter is transported into the deep layers mainly by sinking particles (Volk and Hoffert, 1985). Small (micrometers range) particles settle slowly while large (>100 micrometers) particles are considered to settle more rapidly. Size is an important parameter, determining among others the sinking velocity, mass content and food potential of particles. Particle volume distribution measurements for aggregates in surface water show that most of the mass is encompassed in the 0.1–3 mm range (Jackson et al., 1997). Stemmann et al. (2007) showed that in the size range from microns to millimetres, the volume of large particles can equal the volume of the smaller ones. On the other hand, according to Richardson and Jackson (2007), picoplankton despite their small size (0.2–2.0 μm), may contribute more to oceanic carbon export than currently recognized. Picoplankton can aggregate, be incorporated into settling detritus or consumed as aggregates or as individual cells by higher trophic levels such as the pelagic filter-feeder tunicates or flux-feeder pteropods. These zooplankton short-circuit the microbial loop (Alldredge, 2005; Andersen et al., 1998; Gorsky et al., 1999; Noji et al., 1997) and transform small, slowly settling particles into rapidly sinking large particulate matter (LPM). Organic particles leaving the euphotic zone sink until they are remineralized or reach the ocean bottom. Numerous studies agree that relatively little of the organic matter that leaves the euphotic zone reaches the bottom. Particle flux at 1000 m is considered to be about 10% of that at 100 m (Betzer et al., 1984; Martin et al., 1987; Suess,

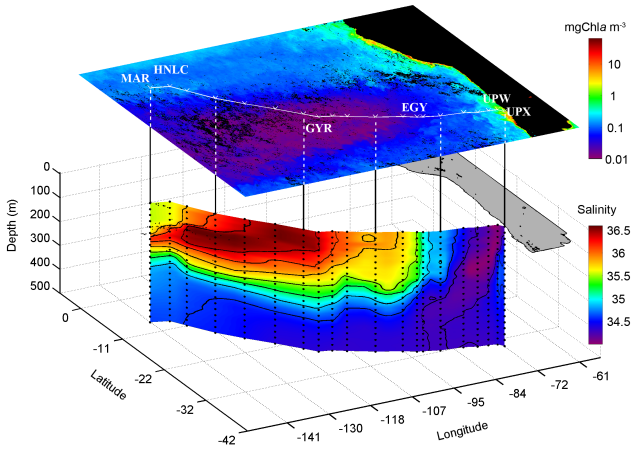

Fig. 1. Salinity section below the BIOSOPE transect superimposed on a SeaWiFS composite image of Chl-*a* concentration. The South American continent is in black and grey. Position of the 6 long-term stations is from left to right: MAR, HNLC, GYR, EGY, UPW and UPX stations.

1980). The decrease in concentration of particles with depth (Bishop and Edmond, 1976; Gardner and Walsh, 1990) implies that intense solubilizing processes of sinking particles occur in the water column during sedimentation. Particles can also be repackaged into larger, faster settling objects with lower concentrations and therefore more difficult to sample.

Estimates of sinking material rely primarily on the deployment of sediment traps (Asper, 1987; Buesseler et al., 2007a; Gardner et al., 2000; Honjo et al., 1984). Problems associated with the use of sediment traps, such as hydrodynamic flushing, swimmer contamination, and sample degradation, make trap measurements difficult to interpret (see Buesseler et al., 2007 for review). One way to increase the reliability of quantitative estimations of vertical export of the particulate matter is to deploy neutrally buoyant traps which drift in the sampled water mass to minimize the bias of advective effects (Buesseler et al., 2007a). In fact, most of the changes in flux with depth occur in the upper 1000 m (Lutz et al., 2002) and most of the processes that can bias flux estimates occur in this layer of the water column. On the other hand, little attention is given in the literature to the role of the particle size distribution although many particle properties fundamental in biogeochemical studies, such as sinking rate and carbon content, depend on accurate determinations of particle size (Burd et al., 2007).

Here we estimate the flux of particles by a method based on optical quantification of particles $>100\,\mu$m (LPM) including the marine snow fraction (Gorsky et al., 2000; Guidi et al., 2007). As this methodology gives a detailed vertical assessment of the LPM abundance and size spectrum, we can estimate fluxes between the surface and the depth of 1000 m (the depth limit of the UVP used during the cruise).

The BIOSOPE (Biogeochemistry and Optics South Pacific Experiment) cruise covered a large range of contrasting hydrodynamic and trophic regimes along an ∼8000 km transect from west of the Marquesas archipelago to the coastal waters of Chile (Claustre et al., 2008, this volume).

On the western end of the BIOSOPE transect, near Marquesas archipelago, an enhancement of the primary production is visible from satellite colour images. This level of production is often due to the island mass effect and has been explained by the dynamic interaction of the circulation and the topography (Martinez and Maamaatuaiahutapu, 2004, and references therein).

The South Pacific Gyre (SPG) is the largest subtropical anticyclonic gyre and the least described region of the ocean (Claustre and Maritorena, 2003; Longhurst, 1995). We know remarkably little about organic matter production and fate in it. The rare observations report very low chlorophyll concentrations (Chavez et al., 1995; Morel et al., 2007).

On the eastern end of the BIOSOPE transect a large biomass is exported offshore and to the deep layers near the Chilean coast fuelled by the Chilean upwelling (Claustre et al., 2008; Thomas, 1999).

The Underwater Video Profiler (UVP, see below for details) was used to assess the particle stock and size spectrum at a high vertical resolution. As part of the BIOSOPE program we fitted the UVP data to sediment trap flux measurements and applied the UVP flux estimations to the 76 profiles made during the BIOSOPE transect. We characterised the distribution of the large particulate matter (LPM) and the resulting fluxes in the 1000-m water column over the whole transect.

2 Methods

2.1 Zone of the study and data acquisition

The BIOSOPE cruise was conducted from 26 October to 11 December 2004. The detailed description of the cruise including the sampling strategy is reviewed in Claustre et al. (2008).

Within this spatial context, we examined the vertical distribution of the Large Particulate Matter (LPM$>100\,\mu$m to 2 cm) using a non-destructive imaging system the Underwater Video Profiler (UVP) constructed in the Laboratoire d'Oceanologie of Villefranche sur mer, France. The vertical deployments were conducted from the surface to the depth of 1000 m (Table 1) at a descent speed of 1 m/s. During the transect, 76 vertical profiles were completed from Marquesas archipelago to the coastal waters of Chile (Fig. 1).

The UVP coupled to a CTD SBE19 (Seabird Inc.) quantified and measured objects illuminated in a slab of water of known volume: 10.53 L. Object sizes are represented by the number of pixels in an image. Size and volume calibrations were conducted in a sea-water tank using natural particles of

Table 1. Location and time of the UVP deployments.

Station	Longitude	Latitude	Date	Time (UT)	Station	Longitude	Latitude	Date	Time (UT)
ES01	−144.001	−12.5	25-Oct-04	1:23 a.m.	STA13	−101.5	−29.09	22-Nov-04	11:31 a.m.
MAR01	−141.14	−8.25	26-Oct-04	1:24 p.m.	STA15	−95.501	−30.42	24-Nov-04	11:34 a.m.
MAR02	−141.16	−8.23	27-Oct-04	10:32 a.m.	STA16	−92.59	−31.25	25-Nov-04	10:18 a.m.
MAR02	−141.16	−8.23	27-Oct-04	11:06 a.m.	EGY02	−91.28	−31.49	26-Nov-04	6:45 a.m.
MAR02	−141.16	−8.22	28-Oct-04	1:45 a.m.	EGY02	−91.27	−31.5	27-Nov-04	3:07 a.m.
MAR02	−141.16	−8.22	28-Oct-04	2:19 a.m.	EGY03	−91.25	−31.52	27-Nov-04	6:07 a.m.
MAR03	−141.16	−8.201	28-Oct-04	10:53 a.m.	EGY03	−91.25	−31.52	27-Nov-04	6:41 a.m.
MAR03	−141.16	−8.201	28-Oct-04	11:27 a.m.	EGY03	−91.24	−31.52	27-Nov-04	7:08 p.m.
MAR04	−141.16	−8.19	29-Oct-04	10:06 a.m.	EGY03	−91.24	−31.52	27-Nov-04	9:05 p.m.
MAR04	−141.16	−8.19	29-Oct-04	10:40 a.m.	EGY03	−91.24	−31.52	27-Nov-04	9:39 p.m.
HLNC01	−136.52	−9.001	31-Oct-04	12:57 p.m.	EGY04	−91.25	−31.52	28-Nov-04	8:54 a.m.
HLNC01	−136.52	−9.01	01-Nov-04	1:25 a.m.	EGY04	−91.25	−31.52	28-Nov-04	9:11 p.m.
HLNC02	−136.53	−9.001	01-Nov-04	10:14 a.m.	EGY04	−91.25	−31.52	28-Nov-04	9:45 p.m.
HLNC02	−136.53	−9.001	01-Nov-04	10:48 a.m.	EGY05	−91.25	−31.54	29-Nov-04	6:18 a.m.
HLNC02	−136.59	−9.03	02-Nov-04	5:09 a.m.	EGY05	−91.25	−31.54	29-Nov-04	6:52 a.m.
HLNC03	−136.58	−9.04	02-Nov-04	10:15 a.m.	EGY05	−91.21	−31.54	29-Nov-04	12:03 p.m.
HLNC03	−136.58	−9.04	02-Nov-04	10:49 a.m.	EGY05	−91.22	−31.53	29-Nov-04	9:49 p.m.
STA01	−134.21	−11.31	03-Nov-04	2:12 p.m.	EGY06	−91.24	−31.54	30-Nov-04	9:07 a.m.
STA03	−130.23	−15.08	05-Nov-04	1:39 p.m.	STA17	−87.26	−32.18	01-Dec-04	10:31 a.m.
STA05	−125.57	−18.301	07-Nov-04	1:36 p.m.	STA18	−84.04	−31.42	02-Dec-04	8:40 p.m.
STA07	−120.51	−21.44	09-Nov-04	1:05 p.m.	STA19	−81.38	−32.57	03-Dec-04	10:25 a.m.
STA09	−116.01	−24.42	11-Nov-04	12:51 p.m.	STA20	−78.22	−33.19	04-Dec-04	10:21 a.m.
GYRE02	−113.59	−26.001	12-Nov-04	11:56 a.m.	STA21	−75.501	−33.35	05-Dec-04	9:57 a.m.
GYRE03	−114.01	−26.001	13-Nov-04	8:16 a.m.	UPW01	−73.23	−33.52	07-Dec-04	1:27 a.m.
GYRE03	−114.01	−26.001	13-Nov-04	8:50 a.m.	UPW02	−73.23	−33.58	07-Dec-04	5:12 a.m.
GYRE03	−114.001	−26.03	13-Nov-04	11:19 p.m.	UPW02	−73.23	−33.58	07-Dec-04	5:46 a.m.
GYRE03	−114.001	−26.03	13-Nov-04	11:53 p.m.	UPW02	−73.24	−33.58	07-Dec-04	8:08 a.m.
GYRE04	−114.02	−26.04	14-Nov-04	10:53 a.m.	UPW02	−73.21	−33.52	07-Dec-04	9:21 p.m.
GYRE04	−114.02	−26.04	14-Nov-04	11:27 a.m.	UPW02	−73.21	−33.52	07-Dec-04	9:55 p.m.
GYRE04	−114.01	−26.05	14-Nov-04	11:20 p.m.	UPW03	−73.18	−33.5	08-Dec-04	6:26 a.m.
GYRE04	−114.01	−26.05	14-Nov-04	11:54 p.m.	UPW03	−73.18	−33.5	08-Dec-04	7:00 a.m.
GYRE05	−114.01	−26.04	15-Nov-04	8:08 a.m.	UPX01	−72.24	−34.32	09-Dec-04	9:03 p.m.
GYRE05	−114.01	−26.04	15-Nov-04	8:42 a.m.	UPX02	−72.26	−34.36	10-Dec-04	1:30 a.m.
GYRE05	−114.01	−26.04	15-Nov-04	9:16 a.m.	UPX02	−72.27	−34.37	10-Dec-04	6:29 a.m.
GYRE05	−114.02	−26.04	15-Nov-04	11:25 p.m.	UPX02	−72.27	−34.37	10-Dec-04	7:03 a.m.
GYRE06	−114.001	−26.04	16-Nov-04	10:28 a.m.	UPX02	−72.301	−34.401	11-Dec-04	1:21 a.m.
STA10	−110.401	−26.51	17-Nov-04	12:22 p.m.	UPX03	−72.29	−34.39	11-Dec-04	8:10 a.m.
STA11	−107.35	−27.42	20-Nov-04	12:17 p.m.	UPX03	−72.29	−34.39	11-Dec-04	8:39 a.m.

different types to determine the conversion between pixels to metric units (Stemmann et al., 2002). Images were recorded digitally at a rate of 12 images per second and processed with custom made image analysis software (Gorsky et al., 2000). The equivalent spherical diameter (ESD) of each particle was calculated assuming that the particle projected shape was a circle.

The resulting particles size distribution and flux data integrated over 5-m intervals were related to the simultaneously acquired CTD and fluorescence data.

This instrument was built for exhaustive optical estimation of

1. the stock of the particles $>100\,\mu$m (large particulate matter – LPM) from the surface to the depth of 1000 m and

2. their size distribution (Stemmann et al., 2007).

We estimated the LPM mass flux along the whole transect. As described more in details in Guidi et al. (2008), we integrated the mass flux over all the particles according to their sizes.

2.2 Flux estimates from the size spectrum of particles

The mass flux was calculated from size spectra using the method from Guidi et al., in press. An extensive set of data with 118 flux measurements from sediment traps (model Technicap PPS5) both moored and drifting and concomitant profiles of aggregate abundance and size distributions were used to parameterize the relationships presented in Guidi et al. (see Table 4 in Guidi et al., in press).

The assumption is that the total mass flux (F) is the mass flux spectrum integrated over all particle sizes. Using diameter (d) as a measure of particle size, then

$$F = \int_0^\infty n(d)m(d)w(d)dd \quad (1)$$

The mass (m) of a spherical particle is given by

$$m(d) = \alpha d^3 \quad (2)$$

where $\alpha = \pi\rho/6$ and ρ is its average density.

Its settling rate (w) can be calculated using Stokes Law as follow:

$$w(d) = \beta d^2 \quad (3)$$

where $\beta = g\,(\rho - \rho_0)(18\upsilon\rho_0)^{-1}$, g is the gravitational acceleration, ρ_0 is the fluid density, and υ is the kinematic viscosity.

If both $w(d)$ and $m(d)$ are given by power relationships, so is the combined quantity,

$$w \cdot m = A \cdot d^b \quad (4)$$

For the above case of constant density (ρ) shown in Eqs. (2) and (3) the exponent b in Eq. (4) is equal to 5. In theory, the spectrum should be integrated over the whole range of particle sizes (i.e. 0 to the effective maximum particle size). In the present study, where the available size range is 100 μm to few cm, the spectrum was calculated over that range.

If the aggregates size distribution and the values of A and b are known, then a mass flux can be calculated from size spectra using Eqs. (1) and (4). The fluxes calculated this way can be compared to matching sediment trap values. Because the appropriate values of A and b are unknown, a minimization procedure was used to find those two values that provided the best fit between the two fluxes: sediment trap and particle size distribution flux derived.

We used the Matlab function fminsearch (The Mathworks, Inc., Natick, MA) to find the values of A and b of Eq. (4) that minimized the log-transformed differences (ΔF_c) between sediment trap and spectral-estimated fluxes:

$$\Delta F_c = \sum_i \left[\log\left(F_{T,i}\right) - \log\left(F_{E,i}\right)\right]^2 \quad (5)$$

where $F_{T,i}$ is the sediment trap flux value and $F_{E,i}$ the associated flux based on Eq. (1) for the ith observation. The logarithmic transformation was used to give equal weight to differences of small and large fluxes.

The minimization procedure yields only one pair of parameter values. We used a jack-knife procedure to estimate the errors of the estimates. The minimization was performed on 1000 subsamples one third the size of the original data set and composed of data pairs selected randomly from the original data set. The results provide us with the frequency distribution of A and b from which mean and standard deviations were calculated (Guidi et al., 2008: Table 4).

Note that the flux integration is only for particles between classes i to m available with the UVP, not the 0–1 shown in Eq. (3).

Hence, knowing A and b (Eq. 4), aggregate with a given size (d) can be directly related to its mass flux. Estimated fluxes with UVP were compared to matching sediment trap observations at global scale. A minimization procedure using the Matlab function fminsearch (Mathworks Inc., Natick, MA) allowed to calculate A and b providing the best fit between the two fluxes, measured from sediment traps and estimated from particle size distributions (Guidi et al., 2008). Residues' normality between model (estimated UVP flux) and data (sediment traps) were tested and the model validated. The mass flux is given in units of dry weight (DW).

2.3 Sediment traps

Drifting surface tethered sediment traps were deployed at all 6 long-term stations (see Fig. 1 and Table 1 for geographical coordinates) for a period of 2 to 4 days. At each site, baffled conical sediment traps model Technicap PPS5 (1 m^2 surface collection) were deployed at 2 depths, ranging from 100–200 m depth at the eastern and western extremities of the cruise transect, to 200–400 m at the center of the South Pacific Gyre. The depth of trap deployments was decided based on the physico-chemical characteristics of the water column. Trap samples were preserved in a 2% formaldehyde solution in ambient seawater to prevent degradation or grazing of the collected particles.

3 Results

3.1 Hydrology

The general hydrology studied during the BIOSOPE cruise is described in Claustre et al. (2008). The surface salinity pattern varied over a large range, from the highly salty waters associated with the South Pacific Tropical Waters (SPTW) around 130° W (salinity of 36.6) towards the Eastern South Pacific Intermediate Water (ESPIW), at 78° W (salinity of ∼34, Fig. 1). The South Equatorial Current (SEC) surrounding the Marquesas Islands (stations MAR) constituted the southern border of High Nutrients Low Chlorophyll (HNLC) waters of the equatorial upwelling region (see Claustre et al.,

2008, and the references herein). The South Pacific gyre (station GYR) was characterized by the strongly stratified Eastern South Pacific Central Waters (ESPCW). East of 100° W, the transition zone between the ESPCW and the waters, influenced by fresher Subantarctic Surface Waters (SASW, Fig. 1), marked the subtropical front. East of EGY stations a tongue of low salinity waters was observed at a depth of 300 m and flowed close to the surface near the coast.

East of 78° W, the ESPIW lies above the relatively saltier Equatorial Subsurface Water (EESW) that extends in the 100–400 m range. The ESPIW is part of the poleward Peru-Chile undercurrent (PCUC, stations UPW, UPX).

3.2 Distribution of the biogeochemical parameters

The distribution and amounts of total chlorophyll-*a* concentration (TChl-*a*) measured along the transect by different methods were similar (Raimbault et al., 2007; Ras et al., 2007). These in situ chlorophyll-*a* measurements matched the values derived from satellite imagery and showed considerable variations along the section. The highest concentrations of Tchl-*a* were recorded in surface layers at the western and eastern extremities; very low chlorophyll content was measured in the centre of the SPG. The lowest concentration occurred near the surface at 114° W (0.02 mg TChl-*a* m^{-3}). Distribution of the in vivo fluorescence of TChl-*a* (Fig. 2) shows the range of variation of the autotrophic biomass along transect.

During the BIOSOPE cruise, the LPM distribution was generally correlated with the vertical distribution of fluorescence (Fig. 3) suggesting a direct relationship between the two parameters. Except the UPX station near the Chilean coast, this relationship was not evident in the deeper layers where the UVP maxima were certainly associated with the detrital or heterotrophic matter. LPM biovolume and abundance were the lowest respectively at the GYR, EGY and HNLC stations while near Chile the water column contained the highest volumes of LPM (Figs. 3 and 4). However, considering only the euphotic zone (see Claustre et al., 2008) the MAR and UPW stations displayed the highest maximum LPM values.

3.3 Sediment trap fluxes

Downward particle flux was very different at the several sites studied and, overall, varied by >2 orders of magnitude between stations. The lowest mass fluxes were measured at the GYR site and at the eastern site of it (2–28 mg m^{-2} d^{-1}) as well as at the HNLC site (11–22 mg m^{-2} d^{-1}). In the more productive waters of MAR particle flux were slightly higher (38–49 mg m^{-2} d^{-1}). In contrast, particle fluxes were significantly higher at the 2 eastern stations off south-America, ranging from 54 to 630 mg m^{-2} d^{-1} at the UPW and UPX sites.

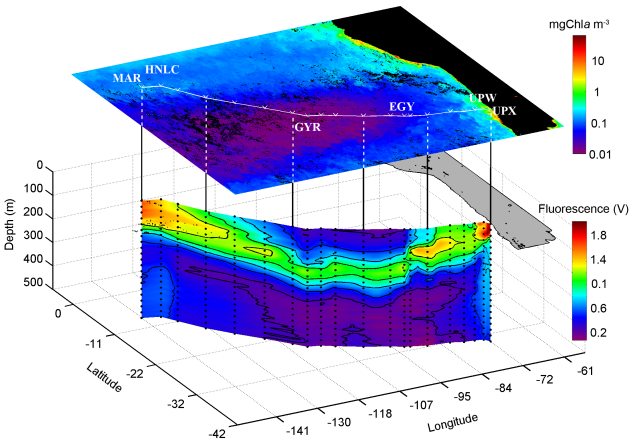

Fig. 2. In vivo fluorescence plot of Chl-*a* along the BIOSOPE section. Note the relatively high values at each end of the transect.

3.4 Comparison of LPM in the distinct zones along the BIOSOPE transect

LPM concentrations along the BIOSOPE transect (Fig. 4) reveal the following features:

1. high abundance of particles in the euphotic zone at the station MAR and relatively high concentration of particles from 150–300 m.
2. deep LPM maximum between 135 and 130° W,
3. a discontinuity in the abundance pattern at the vicinity of 100° W and
4. low particle densities in the low salinity ESPIW water mass (Figs. 1 and 4).

3.4.1 Western portion of the section

The mass flux estimated from size distribution profiles of the LPM along the BIOSOPE transect revealed a strong potential export in the first 150 m at the western end of the transect (Fig. 5). However, below this layer, between 150 and 300 m at the MAR station the LPM vertical flux was very low, forming a discontinuity stratum between the surface and the mesopelagic layers (Fig. 5). Despite the low vertical fluxes at this station (Fig. 5) the abundance of particles was high (Fig. 4). This observation may be explained by the small size and low settling velocities of these particles. The section between MAR and GYR is characterized by the increasing oligotrophy and by the deepening of the nutricline (Raimbault et al., 2007). The deep chlorophyll maximum (DCM) deepens also (Figs. 2 and 3) its base follows the 26 kg m^{-3} isopycnal (Claustre et al., 2008).

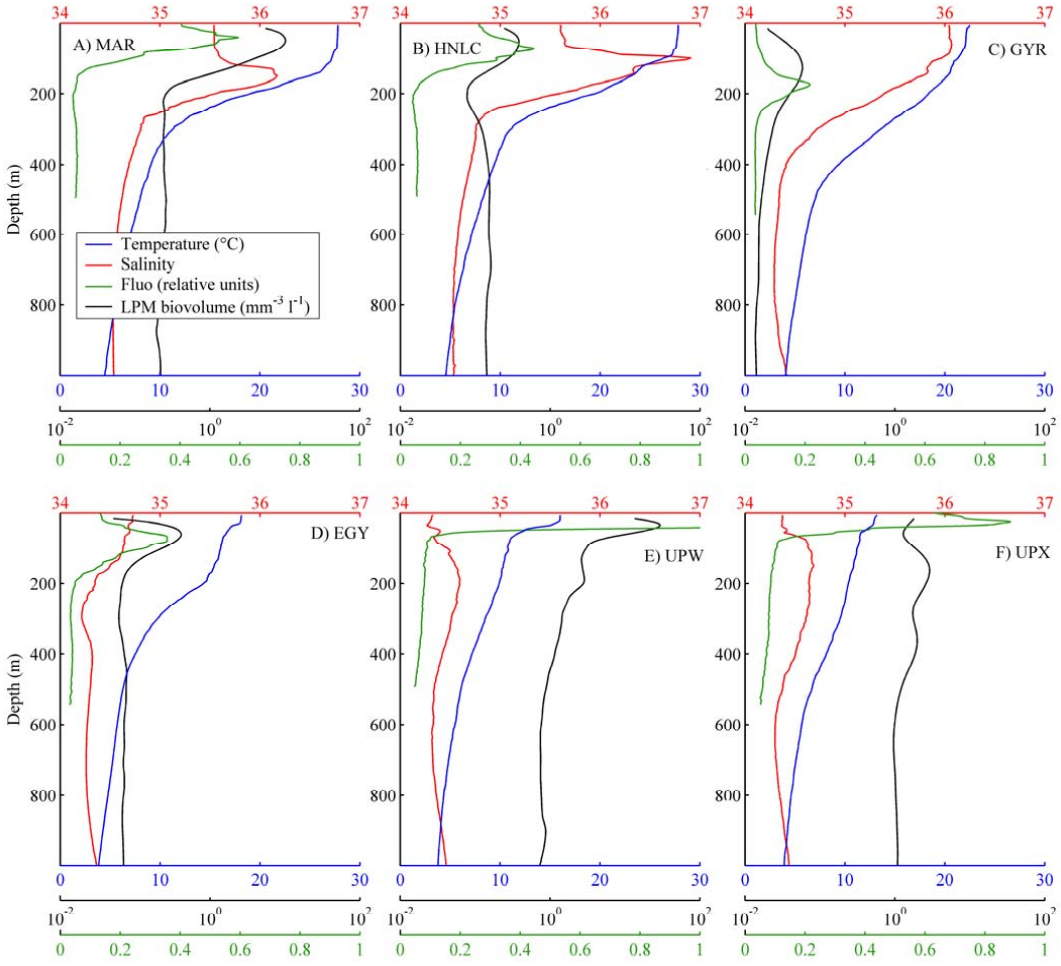

Fig. 3. Mean 0–1000 m profiles of the long-term stations displaying the temperature, salinity, fluorescence (*RU*) and the biovolumes (in $mm^{-3}\,L^{-1}$) of the LPM estimated from the UVP data. Note the logarithmic scale for the LPM data.

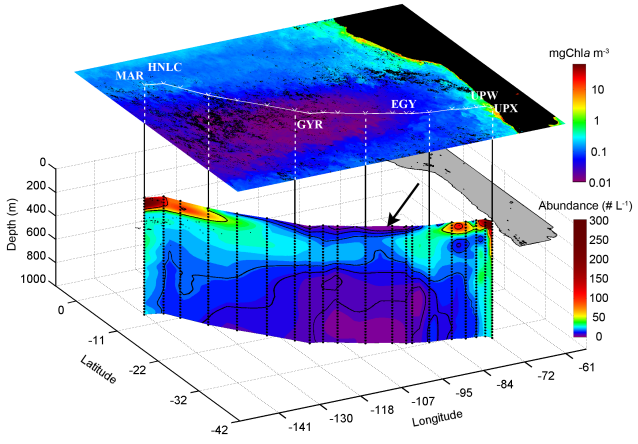

Fig. 4. Abundance of LPM $>100\,\mu$m in the first km of the BIOSOPE cruise. The arrow indicates the discontinuity zone in the abundance distribution of the large particulate matter.

3.4.2 The South Pacific gyre

As expected, the lowest values of particles abundance and the lowest export values were measured in and below the GYR. Abundances were higher in the 100–400-m layer than in the surface. The low biovolume and low fluxes indicate that particles in the SPG were small (Figs. 3 and 5). Eastwards, the strong salinity gradient delineated the limit of the SPG and indicated the presence of the subtropical frontal zone (Fig. 1). A discontinuity in the particle abundance pattern was observed in this zone and the vertical fluxes displayed the lowest values.

3.4.3 Eastern portion of the section

East of the EGY station, and below the ESPIW waters (at a depth of 250 m and below) the water mass had small particle abundance and low vertical flux values. A significant decrease in the concentration of particles was observed at the UPW station in the subsurface layer. Nevertheless, the

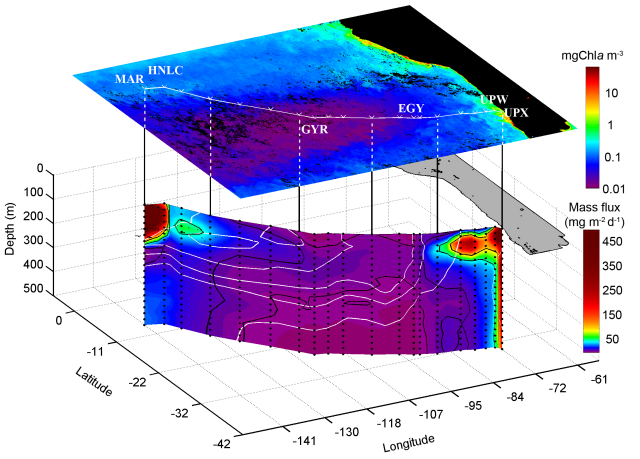

Fig. 5. Mass flux of LPM in mg DW m^{-2} d^{-1} estimated from size measurements of every individual particle recorded during the vertical deployment of the UVP. Only data from 0–500 m are shown for better visualisation of the upper water column structures. The vertical resolution of the sampling was 10.5 L every 8 cm (see Guidi et al., 2007, for details). Isohalines are in white.

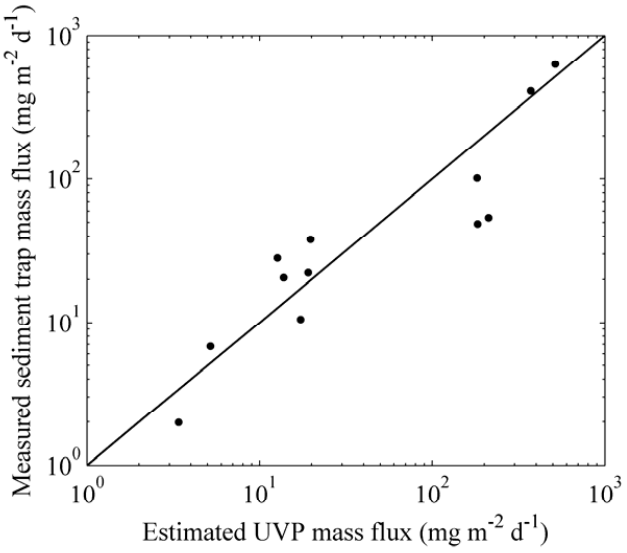

Fig. 6. Drifting sediment trap mass flux measurements versus the UVP estimated mass flux. The sediment traps were deployed below the mixed layer at 2 depths at each site, at 100–200 m depth at the extremities of the transect and at 200–400 m at the centre of the SPG.

particulate volume and vertical export remained high. This result suggests that the contribution of the large particles was high. Near the Chilean coast the mixed layer was reduced and nutrient concentrations and the primary production were high. At the UPX station the Chl-*a* fluorescence signal was measurable even in the intermediate layers. The abundance of particles and the resulting vertical flux was high in the entire water column (Figs. 4 and 5).

4 Discussion

Marine particles vary in length from submicron colloidal particles to marine snow larger than tens of millimeter in diameter (Alldredge and Gotschalk, 1988; Fowler et al., 1987). The abundance of particles varies across this size range, with smaller particles generally being more abundant than larger ones (McCave, 1975). The particle mass however, tends to be concentrated in the larger particles (e.g., Jackson et al., 1997; McCave, 1975).

Here we are using particle diameter to estimate mass and settling rate values. We applied a minimization procedure to find the best fit between the UVP and sediment trap fluxes. Flux estimations made for the 76 UVP profiles were compared to the drifting sediment traps mass flux measurements (Fig. 6) made during the cruise. As the correlation between the optical assessment and the collected matter is good we are applying the flux estimates to all the 76 UVP profiles providing extensive information on the potential export in the different depths along the whole transect. Image acquisition is a conservative sampling method. With the improvement of the sediment trap methodology sensu Buesseler et al. (2007b) we will be able to ameliorate also the trap-UVP correlations and provide more precise flux data with high spatial and temporal resolution. This treatment can be done retrospectively and also on past data stored in the UVP databank (http://www.obs-vlfr.fr/LOV/ZooPart/UVP/).

4.1 Abundance vs. fluxes

4.1.1 Western portion of the section

On the western end of the BIOSOPE transect, (station MAR), the abundance of particulate matter in the surface zone is very high (Fig. 4). According to Gomez (2007), the small pennate cluster forming diatom *Pseudo-nitzschia delicatissima* and the large centric diatom *Rhizosolenia bergonii* were the main microphytoplanktonic constituents of this layer. Large, rapidly sinking phytoplankton, such as diatoms, are believed to control carbon flux from upper ocean layers (Michaels and Silver, 1988). However as pointed out by Gomez (2007) in the western and eastern part of the BIOSOPE transect, the surface layer diatom population was characterized by frustules with low silicate content because of the silicate-limited environment. This feature may also limit their ballasting efficiency.

Although the abundance profile shows a vertical continuum and the surface LPM maximum is the second highest on the whole transect (Fig. 4), the flux estimations calculated from the UVP data fitted to the drifting sediment trap measurements reveal that the export between 150 and 250 m is very low (Fig. 5). This discontinuity in the vertical flux

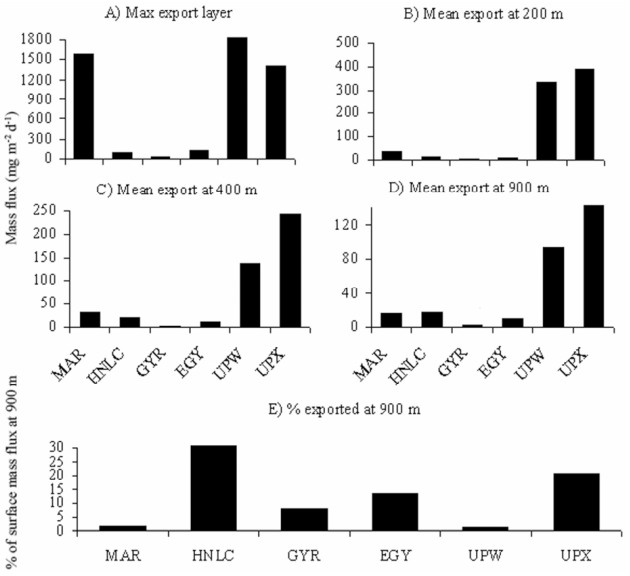

Fig. 7. Mean export at different depths and the % exported below 900 m related to the potential surface export maximum (UVP data fitted to sediment trap measurements).

clearly observed at the station MAR may be the result of different biological and physical factors. Large unknown transparent objects were detected by the UVP at the MAR site (see Fig. 7 in Stemmann et al., 2007). These circular-shaped objects were about 2–5 mm in diameter with concentrations between 1–10 objects L^{-1}. They were located throughout the upper 200 m but below 170 m their concentration decreased. If they were anomalous, low-density organism, they might increase the apparent flux values in the upper layer. Below, the particles population was composed of small size classes. The hydrology at the MAR site may also contribute to the discontinuity in the vertical export. The discontinuity stratum (150–250 m) corresponds to the zone of narrowing density field and is the site of strong advective processes (Figs. 3 and 4 in Claustre et al., 2008). These advective processes may be responsible of the change in the size structure of the particles population. Below this discontinuity layer the vertical flux values increase slightly. This feature is clearly visible in the Fig. 7.

An increase of the LPM flux was observed in the HNLC zone in the vicinity of 130° W. This increase may be associated with the deepening of the sub-surface isotherms (Claustre et al., 2008). About 30% of the maximum surface layer flux was observed below 900 m at the HNLC station. In fact, the mean export initially decreased at 200 m when compared to the maximum flux at the surface layer, but then it increased with depth (Figs. 3 and 7). The surface production at this region is weak: only about 99 mg m^{-2} d^{-1} in the maximum layer, but still about 20 mg m^{-2} d^{-1}below 900 m. The reason for the increase of exported mass at depth may be linked to other processes such as aggregation, advection or to the low oxygen conditions. Furthermore, no significant difference was observed between the day and night fluxes that may be attributed to the vertical zooplankton migration (Stemmann et al., 2007). According to Claustre et al. (2008) in this area the currents were weak. Therefore, the hypothesis that the increase of large particles flux may be associated with suboxic conditions should be further explored. According to Claustre et al. (2008) this oxygen minimum reflects the signature of north-westwards propagation of the oxygen minimum zone developed along South America. Typically, these zones underlie regions of high biological productivity and thus high production of organic matter. The transition from oxic to anoxic conditions involves important biogeochemical shifts. In the absence of oxygen, nitrate is used to oxidize organic material (Stramma et al., 2008). Oxygen-poor conditions have far-reaching impacts on ecosystems because important mobile macroorganisms avoid or cannot survive in hypoxic zones. It is hypothesized that low oxygen is limiting the vertical migration of zooplankton (Morrison et al., 1999) and thus the fragmentation processes. This is a region of denitrification, and the presence and activities of bacteria may cause the increase in particles. On the other hand, the suboxic conditions might prevent the degradation of particulate matter. This hypothetical particle preservation could also occur in the Marquesas area. Below 200 m there is a good conservation of the mass flux. Mass flux estimated at 900 m is 70% of mass flux estimated at 200 m.

4.1.2 The South Pacific gyre

The SPG is known as a hyper-oligotrophic water mass (Claustre and Maritorena, 2003; Morel et al., 2007). The biological production in the surface zone is the lowest in the global ocean. Peaks of small particles centered at 100 m were associated with a *Prochlorococcus* sp. population (Grob et al., 2007). The deep chlorophyll maximum (DCM) located between 160–200 m was mainly composed of picophytoeukaryotes, although some coccolithophorid and diatom cells were also present (Beaufort et al., 2007; Gomez et al., 2007; Ras et al., 2007). The maximum phaeophorbide (a tracer for altered Chl-*a*) concentration was found also in this layer (Ras et al., 2007). Oligotrophic regions, where small cells dominate the production, can contribute significantly to the global carbon flux via detritus (Richardson and Jackson, 2007). The mass flux associated with the DCM was estimated from the UVP data as $\sim$30 mg m^{-2} d^{-1}. The export at 200 m was 20% of that in surface waters and about 8% at 900 m ($\sim$2 mg m^{-2} d^{-1}). While considering the large geographical extent of the SPG, this extreme oligotrophic ecosystem is producing a non negligible amount of carbon. Due to the lack of seasonal vertical mixing and weak lateral advection, the biologically produced LPM carbon can be exported and trapped in the deep layers for long periods.

4.1.3 Eastern portion of the section

In the vicinity of 100° W, we observe a distinct discontinuity in the abundance distribution of the LPM (arrow in Fig. 4). This discontinuity corresponds to the uplifted isolines delineating the subtropical front as described in Claustre et al. (2008). At EGY, the DCM is located at the depth of 80 m but the export values are low, similar to the HNLC station. The mean surface layer maximum export is estimated as 127 mg m^{-2} d^{-1}, and a slight increase of fluxes with depth can be observed (Fig. 7). About 13% of the surface export is measured below 900 m. This result constitutes 94% of the vertical flux estimated at 200 m. No difference was observed between the day and night fluxes.

The situation is quite different off and near the Chilean coast. High LPM concentrations are observed in the surface zone with a strong decrease below at the location of the low salinity waters (Fig. 1). This feature is not detected on the flux plot (Fig. 5). Therefore, the decrease in abundance is related to the small particle fraction. At the UPW station, the situation changed. The potential export from the Chl-*a* maximum estimated for the whole section is 7367 mg m^{-2} d^{-1}. At depths of 200 m and 900 m only 4.6% and 1.5% respectively of this flux remained. Thus, 95% of the matter was remineralized, disaggregated to $<100\,\mu$m or advected. At both coastal stations the vertical zooplankton migration was significant. Near the Chilean coast, at the UPX stations, the vertical flux remained high in the entire water column. The surface maximum export was 1400 mg m^{-2} d^{-1}, lower than the mean UPW surface maximum but in contrary to the latter, 20% of the surface layer flux was observed below 900 m (Fig. 7). Thus the remineralization processes differ in the two stations near the Chilean coast.

4.2 Export efficiency

Particulate export is a result of particle supply, production, consumption and aggregation/disaggregation. These processes are developed at different scales of variability including time lags between biological production and export. During settling, particles disaggregate, decompose and disappear. Some of the marine snow particles may be fragmented by the swimming activity of migrating zooplankton (Dilling and Alldredge, 2000; Goldthwait et al., 2004). Most are transformed into particles smaller than the 100 μm cutoff of the UVP and/or into dissolved matter by the processes of remineralization. Some may coalesce into larger particles by grazing or aggregation (Alldredge and Silver, 1988; Jackson and Burd, 2002). It is at depths between the surface euphotic zone and roughly 1000 m where most sinking particles are remineralized (Buesseler et al., 2007b). The variety of vertical profiles shows that there are variations in remineralization rates or advection rates with depth. Blooms of some species, like coccolithophores or diatoms and the consequent phytodetritus deposition, can cause episodic changes in remineralization length-scales (Nodder et al., 2007); blooms of filter-feeder thaliaceans, larvaceans or flux-feeder pteropods can change element ratios, sinking speeds and ballasting (Alldredge, 2005; Andersen et al., 1998; Boyd and Newton, 1995) or size distributions of particles (Gorsky et al., 1999). Zooplankton affect particle flux in the sea in a number of ways; they create or aggregate particles by feeding and producing sinking fecal pellets, disaggregate sinking particles by their feeding or swimming activities, remineralize sinking particles through their feeding and metabolism, and actively transport particulate and dissolved organic matter from the surface to depth by vertical migration (e.g., Fowler et al., 1987; Longhurst et al., 1990). Beyond the overall changes in particle flux with depth, changes in composition of the sinking material can have an impact on carbon gradients. Steinberg et al. (2008), compared losses of sinking POC measured by neutrally buoyant sediment traps with bacteria and zooplankton metabolic requirements in the subtropical Pacific and in the subarctic Pacific. Mesopelagic bacterial carbon demand was respectively 3- to 4-fold, and 10-fold greater than the loss of sinking POC flux, while zooplankton carbon demand was 1- to 2-fold, and 3- to 9-fold greater. Nevertheless, on the studied section and in the different trophic regimes UVP data indicate that particle export below 900 m was not negligible.

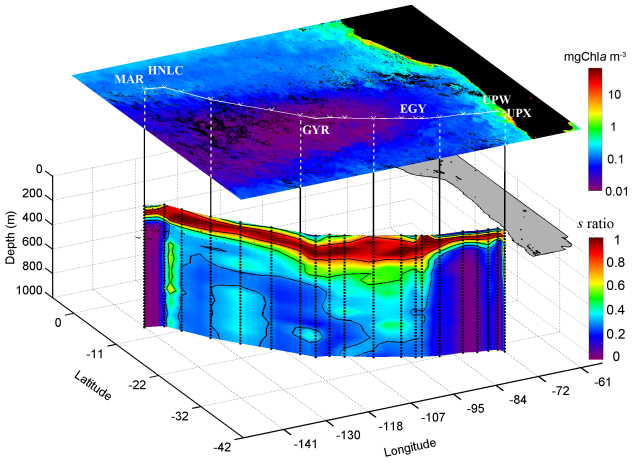

Fig. 8. The s ratio corresponding to the LPM mass flux (F) estimated at depth Z normalized by the flux estimated below Ze (s-ratio (Z)=$F(Z)/F(Ze)$). Here, Ze is the depth where the mass flux is maximal (s-ratio is equal to 1 for Ze: dark red).

During the BIOSOPE transects in the different geographic zones the relative fluxes when compared to the surface maximums were different (Fig. 8). Higher proportion of particulate matter was mediated to the deep layers in the GYR region than in the rich surface layer MAR or UPW zones.

Sinking velocities determine the depth at which remineralization occurs, which in turn determines how soon remineralized nutrients and carbon will be returned to the surface

ocean (Sarmiento and Gruber, 2006). Particles of the same excess density settle at roughly the same speed principally because Reynolds number is very sensitive to particle size (Khelifa and Hill, 2006a, b). Although organic compounds are initially present in different proportions in the particles with different settling velocities, the degradation process can lead to uniform chemical compositions of particles (Goutx et al., 2007). This change reflects the processes of loss through enzymatic hydrolysis of source compounds and input of bacterial biomass. The settling speed may differ in the different regions due to the differences in the composition of primary and secondary producers. More studies should test the hypothesis on which our flux estimations are based, i.e., that at mesopelagic depths particles of similar size settle at a more or less uniform speed due to their similar composition.

5 Conclusions

Abundance and size spectrum of particles $>100\ \mu$m were optically estimated from the surface to 1000 m and the mass flux of particles was calculated. The resulting mass fluxes estimated with the UVP were compared to drifting sediment trap data (at the 6 locations) and applied over the whole BIOSOPE transect.

The LPM abundance and the estimated fluxes varied considerably across the study area. At the MAR station the abundance profile showed a vertical continuum while the vertical flux decreased significantly between 150 and 250 m. This change could be due to an abundance of large, unidentified low-density objects that disappeared with depth, or due to intense hydrodynamic processes (Figs. 3 and 4 in Claustre et al., 2008) in this zone. Only about 2% of the upper zone LPM was exported below 900 m.

Contrastingly, about 30% of the maximum surface flux was observed below 900 m at the HNLC station. This feature may be associated with the suboxic conditions (Claustre et al., 2008).

In spite of relatively small values (2% of the surface layer maximum), the carbon export below the extreme oligotrophic SPG is not negligible. The lack of seasonal vertical mixing and weak lateral advection suggest that this material can be trapped in deep layers for long periods.

A discontinuity in the abundance distribution of the LPM is observed in the vicinity of 100° W and is associated with the intrusion of the subtropical front.

High LPM concentrations are observed in the upper layer off and near the Chilean coast. There is a strong decrease of particles abundance below this layer in the low salinity waters, but not in the vertical flux, suggesting a decrease in the small particle population only.

The potential export from the Chl-*a* maximum displays the highest value at the UPW station but at depths of 200 m and 900 m, only 4.6% and 1.5% respectively of this flux remains. 95% of the matter is remineralized, disaggragated or advected away.

At the UPX station, the vertical flux remains high in the entire water column. In contrast to UPW, 20% of the surface flux is still observed below 900 m.

Variations in the estimated flux rates of LPM obtained in this study suggest that a wide variety of biotic and abiotic processes may drive the aggregation-disaggregation processes and influence the export of matter from mesopelagic layers. This conclusion suggests that LPM export to deep waters is heterogeneous and that optical methods allowing high spatial resolution studies should be utilized in deep sea habitats.

Acknowledgements. This work was supported by the French national programs LEFE and PNEC (ZOOPNEC project). Special thanks to the crew of the ATALANTE French oceanographic vessel for their assistance with this research. We thank the two anonymous referees for the substantial improvement of the ms and M. Youngbluth for constructive discussions. The International Atomic Energy Agency is grateful for the support provided to its Marine Environment Laboratories by the Government of the Principality of Monaco.

Edited by: T. J. Battin

References

Alldredge, A.: The contribution of discarded appendicularian houses to the flux of particulate organic carbon from oceanic surface waters, in: Response of marine ecosystems to global change: Ecological impact of appendicularians, edited by: Gorsky, G., GB Science Publishers-Editions Scientifiques GB, Paris, 309–326, 2005.

Alldredge, A. L. and Gotschalk, C.: In situ settling behavior of marine snow, Limnol. Oceanogr., 33, 339–351, 1988.

Alldredge, A. L. and Silver, M. W.: Characteristics, dynamics and significance of marine snow, Prog. Oceanogr., 20, 41–82, 1988.

Andersen, V., Francois, F., Sardou, J., Picheral, M., Scotto, M., and Nival, P.: Vertical distributions of macroplankton and micronekton in the ligurian and tyrrhenian seas (northwestern mediterranean), Oceanol. Acta, 21, 655–676, 1998.

Asper, V. L.: Measuring the flux and sinking speed of marine snow aggregates, Deep-Sea Res. Pt. I, 34, 1–17, 1987.

Beaufort, L., Couapel, M., Buchet, N., and Claustre, H.: Calcite production by Coccolithophores in the South East Pacific Ocean: from desert to jungle, Biogeosciences Discuss., 4, 3267–3299, 2007.

Betzer, P. R., Showers, W. J., Laws, E. A., Winn, C. D., Ditullio, G. R., and Kroopnick, P. M.: Primary productivity and particle fluxes on a transect of the equator at 153-degrees-w in the pacific-ocean, Deep-Sea Res. Pt. I, 31, 1–11, 1984.

Bishop, J. K. B. and Edmond, J. M.: A new large volume filtration system for the sampling of oceanic particulate matter, J. Mar. Res., 34, 181–198, 1976.

Boyd, P. and Newton, P.: Evidence of the potential influence of planktonic community structure on the interannual variability of

particulate organic-carbon flux, Deep-Sea Res. Pt. I, 42, 619–639, 1995.

Buesseler, K. O., Antia, A. N., Chen, M., Fowler, S. W., Gardner, W. D., Gustafsson, O., Harada, K., Michaels, A. F., van der Loeff, M. R., Sarin, M., Steinberg, D. K., and Trull, T.: An assessment of the use of sediment traps for estimating upper ocean particle fluxes, J. Mar. Res., 65, 345–416, 2007a.

Buesseler, K. O., Lamborg, C. H., Boyd, P. W., Lam, P. J., Trull, T. W., Bidigare, R. R., Bishop, J. K. B., Casciotti, K. L., Dehairs, F., Elskens, M., Honda, M., Karl, D. M., Siegel, D. A., Silver, M. W., Steinberg, D. K., Valdes, J., Van Mooy, B., and Wilson, S.: Revisiting carbon flux through the ocean's twilight zone, Science, 316, 567–570, 2007b.

Burd, A. B., Jackson, G. A., and Moran, S. B.: The role of the particle size spectrum in estimating poc fluxes from 234th/238u disequilibrium, Deep-Sea Res. Pt. I, 54, 897–918, 2007.

Chavez, F. P., Buck, K. R., Bidigare, R. R., Karl, D. M., Hebel, D., Latasa, M., Campbell, L., and Newton, J.: On the chlorophyll-*a* retention properties of glass-fiber gf/f filters, Limnol. Oceanogr., 40, 428–433, 1995.

Claustre, H. and Maritorena, S. The many shades of ocean blue, Science, 302, 1514–1515, 2003.

Claustre, H., Sciandra, A., and Vaulot, D.: Introduction to the special section bio-optical and biogeochemical conditions in the South East Pacific in late 2004: the BIOSOPE program, Biogeosciences, 5, 679–691, 2008. [redacted]**BG update inserted!**

Fowler, S. W., Buat-Menard, P., Yokoyama, Y., Ballestra, S., Holm, E., and Van Nguyen, H.: Rapid removal of chernobyl fallout from mediterranean surface waters by biological activity, Nature, 329, 56–58, 1987.

Dilling , L. and Alldredge, A. Fragmentation of marine snow by swimming macrozooplankton: A new process impacting carbon cycling in the sea. Deep-Sea Res. Pt. I, 47, 1227–1245, 2000.

Gardner, W. D. and Walsh, I. D.: Distribution of macroaggregates and fine-grained particles across a continental-margin and their potential role in fluxes, Deep-Sea Res. Pt. I, 37, 401–411, 1990.

Gardner, W. D., Richardson, M. J., and Smith, W. O.: Seasonal patterns of water column particulate organic carbon and fluxes in the ross sea, antarctica, Deep-Sea Res. Pt. II, 47, 3423–3449, 2000.

Goldthwait, S., Yen, J., Brown, L., and Alldredge, A.: Quantification of marine snow fragmentation by swimming euphausiids, Limnol. Oceanogr., 49, 940–952, 2004.

Gomez, F.: On the consortium of the tintinnid eutintinnus and the diatom chaetoceros in the Pacific ocean, Mar. Biol., 151, 1899–1906, 2007.

Gorsky, G., Chretiennot-Dinet, M. J., Blanchot, J., and Palazzoli, I.: Picoplankton and nanoplankton aggregation by appendicularians: Fecal pellet contents of megalocercus huxleyi in the equatorial pacific, J. Geophys. Res.-Oceans, 104, 3381–3390, 1999.

Gorsky, G., Picheral, M., and Stemmann, L.: Use of the underwater video profiler for the study of aggregate dynamics in the north mediterranean, Estuar. Coast. Shelf Sci., 50, 121–128, 2000.

Goutx, M., Moriceau, B., Lee, C., Liu, Z., Guigue, C., Duflos, M., Tedetti, M., Sempere, R., Wakeham, S. G., and Xue, J.: Composition and degradation of marine particles with different settling velocities, Limnol. Oceanogr., 52(4), 1645–1664, 2007.

Grob, C., Ulloa, O., Claustre, H., Huot, Y., Alarcón, G., and Marie, D.: Contribution of picoplankton to the total particulate organic carbon concentration in the eastern South Pacific, Biogeosciences, 4, 837–852, 2007.

Guidi, L., Stemmann, L., Legendre, L., Picheral, M., Prieur, L., and Gorsky, G.: Vertical distribution of aggregates ($>110\,\mu$m) and mesoscale activity in the northeastern atlantic: effects on the deep vertical export of surface carbon, Limnol. Oceanogr., 52, 7–18, 2007.

Guidi, L., Jackson, G. A., Stemmann, L., Miquel, J. C., Picheral, M., and Gorsky, G.: Relationship between particle size distribution and flux in the mesopelagic zone, Deep-Sea Res. Pt. I, [redacted]**please specify volume and article number.**, doi:10.1016/j.dsr.2008.05.014, 2008.

Honjo, S., Doherty, K. W., Agrawal, Y. C., and Asper, V. L.: Direct optical assessment of large amorphous aggregates (marine snow) in the deep ocean, Deep-Sea Res. Pt. I, 31, 67–76, 1984.

Jackson, G. A., Maffione, R., Costello, D. K., Alldredge, A. L., Logan, B. E., and Dam, H. G.: Particle size spectra between 1 μm and 1 cm at Monterey Bay determined using multiple instruments, Deep-Sea Res. Pt. I, 44, 1739–1767, 1997.

Jackson, G. A. and Burd, A. B.: A model for the distribution of particle flux in the mid-water column controlled by subsurface biotic interactions, Deep-Sea Res. Pt. II, 49, 193–217, 2002.

Khelifa, A. and Hill, P. S.: Models for effective density and settling velocity of flocs, J. Hydraul. Res., 44, 390–401, 2006a.

Khelifa, A. and Hill, P. S.: Kinematic assessment of floc formation using a monte carlo model, J. Hydraul. Res., 44, 548–559, 2006b.

Longhurst, A.: Seasonal cycles of pelagic production and consumption, Prog. Oceanogr., 36, 77–167, 1995.

Longhurst, A. R., Bedo, A. W., Harrison, W. G., Head, E. J. H., and Sameoto, D. D.: Vertical flux of respiratory carbon by oceanic diel migrant biota, Deep-Sea Res., 37, 685–694, 1990.

Lutz, M., Dunbar, R., and Caldeira, K.: Regional variability in the vertical flux of particulate organic carbon in the ocean interior, Global Biochem. Cy., 16, 1–15, 2002.

Martin, J. H., Knauer, G. A., Karl, D. M., and Broenkow, W. W.: Vertex: carbon cycling in the Northeast Pacific, Deep-Sea Res., 34, 267–285, 1987.

Martinez, E. and Maamaatuaiahutapu, K.: Island mass effect in the marquesas islands: Time variation, Geophys. Res. Lett., 31, L18307, doi:10.1029/2004GL020682, 2004.

McCave, I. N.: Vertical flux of particles in the ocean, Deep-Sea Res., 22, 491–502, 1975.

Michaels, A. F. and Silver, M. W.: Primary production, sinking fluxes and the microbial food web, Deep-Sea Res., 35, 473–490, 1988.

Morel, A., Gentili, B., Claustre, H., Babin, M., Bricaud, A., Ras, J., and Tieche, F.: Optical properties of the "Clearest" Natural waters, Limnol. Oceanogr., 52, 217–229, 2007.

Morrison, J. M., Codispoti, L. A., Smith, S. L., Wishner, K., Flagg, C., Gardner, W. D., Gaurin, S., Naqvi, S. W. A., Manghnani, V., Prosperie, L., and Gundersen, J. S.: The oxygen minimum zone in the Arabian Sea during 1995, Deep-Sea Res. Pt. II, 46, 1903–1931, 1999.

Nodder, S. D., Duineveld, G. C. A., Pilditch, C. A., Sutton, P. J., Probert, P. K., Lavaleye, M. S. S., Witbaard, R., Chang, F. H., Hall, J. A., and Richardson, K. M.: Focusing of phytodetritus deposition beneath a deep-ocean front, Chatham rise, New Zealand, Limnol. Oceanogr., 52, 299–314, 2007.

Noji, T. T., Bathmann, U. V., von Bodungen, B., Voss, M., Antia,

A., Krumbholz, M., Klein, B., Peeken, I., Noji, C. I. M., and Rey, F.: Clearance of picoplankton-sized particles and formation of rapidly sinking aggregates by the pteropod, limacina retroversa, J. Plankton Res., 19, 863–875, 1997.

Raimbault, P., Garcia, N., and Cerutti, F.: Distribution of inorganic and organic nutrients in the South Pacific Ocean – evidence for long-term accumulation of organic matter in nitrogen-depleted waters, Biogeosciences, 5, 281–298, 2008. [redacted]**BG update inserted!**

Ras, J., Claustre, H., and Uitz, J.: Spatial variability of phytoplankton pigment distributions in the Subtropical South Pacific Ocean: comparison between in situ and predicted data, Biogeosciences, 5, 353–369, 2008. [redacted]**BG update inserted!**

Richardson, T. L. and Jackson, G. A.: Small phytoplankton and carbon export from the surface ocean, Science, 315, 838–840, 2007.

Sarmiento, J. L. and Gruber, N.: Ocean Biogeochemical Dynamics, Princeton University Press, Princeton, Woodstock, UK, 503 pp., 2006.

Steinberg, D. K., Van Mooy, B. A. S., Buesseler, K. O., Boyd, P. W., Kobari, T., and Karl, D. M.: Microbial vs. zooplankton control of sinking particle flux in the ocean's twilight zone, Limnol. Oceanogr., in press, 2008. [redacted]**update?**

Stemmann, L., Gorsky, G., Marty, J. C., Picheral, M., and Miquel, J. C.: Four-year study of large-particle vertical distribution (0–1000 m) in the nw mediterranean in relation to hydrology, phytoplankton, and vertical flux, Deep-Sea Res. Pt. II, 49, 2143–2162, 2002.

Stemmann, L., Eloire, D., Sciandra, A., Jackson, G. A., Guidi, L., Picheral, M., and Gorsky, G.: Volume distribution for particles between 3.5 to 2000 μm in the upper 200 m region of the South Pacific Gyre, Biogeosciences, 5, 299–310, 2008. [redacted]**BG update inserted!**

Stramma, L., Johnson, G. C., Sprintall, J., and Mohrholz, V.: [redacted]**title?**, Science, 320, 655–658, 2008.

Suess, E.: Particulate organic-carbon flux in the oceans – surface productivity and oxygen utilization, Nature, 288, 260–263, 1980.

Thomas, A. C.: Seasonal distributions of satellite-measured phytoplankton pigment concentration along the Chilean coast, J. Geophys. Res.-Oceans, 104, 25 877–25 890, 1999.

Volk, T. and Hoffert, M. I.: Ocean carbon pumps: analysis of relative strengths and efficiencies in ocean-driven atmospheric CO_2 changes, in: The carbon cycle and atmospheric CO_2: natural variations archean to present, Proceedings of the Chapman Conference on Natural Variations in Carbon Dioxide and the Carbon Cycle, Tarpon Springs, FL, USA, 9–13 January 1984, A86-39426 18–46, 1985.